

Performance Bounds of Near-Field Sensing with Circular Arrays

Zhaolin Wang*, Xidong Mu*, and Yuanwei Liu*

*Queen Mary University of London, London, UK.

E-mail: {zhaolin.wang, xidong.mu, yuanwei.liu}@qmul.ac.uk

Abstract—The performance bounds of near-field sensing are studied for circular arrays, focusing on the impact of bandwidth and array size. The closed-form Cramér-Rao bounds (CRBs) for angle and distance estimation are derived, revealing the scaling laws of the CRBs with bandwidth and array size. Contrary to expectations, enlarging array size does not always enhance sensing performance. Furthermore, the asymptotic CRBs are analyzed under different conditions, unveiling that the derived expressions include the existing results as special cases. Finally, the derived expressions are validated through numerical results.

I. INTRODUCTION

Multiple-input multiple-output (MIMO) has played a critical role in wireless sensing systems [1] and has also been regarded as a key enabling technology for integrating wireless sensing functionalities into the mobile communication networks [2]. The current fifth-generation (5G) wireless network is based on the massive MIMO concept, which was first introduced by Marzetta in 2010 [3]. A typical 5G massive MIMO base station (BS) would be equipped with 64 antennas. Looking forward to the sixth-generation (6G) era in the 2030s, the new concepts of extremely large-scale MIMO (XL-MIMO) and extremely large-aperture antenna array (ELAA), which may include hundreds or even thousands of antennas, have been proposed and received growing attention [4], [5]. This will not only increase the aperture size of antenna arrays but also bring about fundamental changes to the electromagnetic properties of wireless signals [6]. In particular, as the array aperture grows, the near-field region around BSs can be greatly expanded. Such expansion can be more significant in the high-frequency bands, such as millimeter wave and terahertz bands. Generally speaking, in the near-field region, the spherical-wave propagation of wireless signals is dominant, which is fundamentally different from the planar-wave propagation observed in far-field scenarios. Therefore, it is crucial to reevaluate the wireless sensing performance from a near-field perspective.

There are two key factors determining wireless sensing performance: *bandwidth* and *array size*. In conventional far-field sensing, these factors are primarily associated with the resolution of *distance* and *angle* estimation, respectively [7]. However, in near-field sensing, the array size not only affects the resolution of angle estimation but also impacts distance estimation due to spherical-wave propagation, thus alleviating the stringent requirement on bandwidth. This unique advantage motivates extensive studies on near-field sensing performance in narrowband systems, disregarding the influence of bandwidth [8]–[11]. Additionally, while most existing studies focus

on uniform linear arrays (ULAs), the effective array aperture of ULAs significantly diminishes near the edges, which can severely impair sensing performance at large incident and departure angles. Circular arrays have been proven to be a promising solution to address this challenge due to their isotropic radiation properties [12], [13].

Against the above background, this paper studies the joint impact of bandwidth and array size on near-field sensing performance with circular arrays. The analysis is based on the widely exploited Cramér-Rao bound (CRB) framework [8]–[11] and the most popular orthogonal frequency-division multiplexing (OFDM) wideband signaling method [14]. Based on these preconditions, we derive closed-form expressions for the CRBs of angle and distance estimation, which unveil the joint effects of bandwidth and array size on near-field sensing performance. We further explore the asymptotic behavior of these CRBs under various scenarios to elucidate the connections between our new findings and existing literature. Finally, numerical results are provided to validate the analytical results.

II. SYSTEM MODEL

We study near-field sensing in a legacy wideband OFDM system with an N -antenna base station (BS). The BS carries out mono-static sensing for a point target located within the near-field region of the BS. We assume a shared uniform circular array (UCA) for transmitting and receiving at the BS through the use of circulators and the perfect self-interference cancellation through the full-duplex techniques.

A. Transmit Signal Model

Consider an OFDM frame with L OFDM symbols. Let f_c denote the carrier frequency, M denote the number of subcarriers, T_s denote the elementary duration of an OFDM symbol, and T_{cp} denote the duration of the cyclic prefix (CP). Consequently, the subcarrier spacing, the overall bandwidth, and the overall symbol duration of the OFDM system are $\Delta f = \frac{1}{T_s}$, $B = M\Delta f$, and $T_{tot} = T_s + T_{cp}$, respectively. Then, the baseband transmit signal over an OFDM frame can be expressed as [14]

$$\bar{\mathbf{x}}(t) = \frac{1}{\sqrt{M}} \sum_{l=0}^{L-1} \sum_{m=0}^{M-1} \mathbf{x}_{l,m} e^{j2\pi\delta_m\Delta f t} \text{rect}\left(\frac{t - lT_{tot}}{T_{tot}}\right), \quad (1)$$

where $\mathbf{x}_{l,m} \in \mathbb{C}^{N \times 1}$ denotes the data signal on the m -th subcarriers in the l -th OFDM symbol, $\text{rect}(t)$ denotes the rectangular function which has a value of 1 if $t \in [0, 1]$

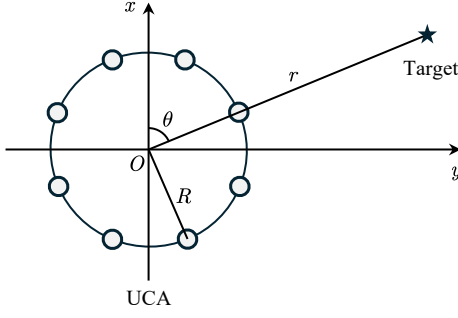


Fig. 1: Geometry of the considered system.

and 0 otherwise, and $\delta_m = \frac{2m-M+1}{2}$. The covariance matrix of signal $\mathbf{x}_{l,m}$ is defined as $\mathbf{R}_m = \mathbb{E}[\mathbf{x}_{l,m}\mathbf{x}_{l,m}^H] \succeq 0$. In this paper, we consider the average power constraint for each subcarrier, which is given by $\text{tr}(\mathbf{R}_m) \leq P$, with P being the transmit power budget for a single subcarrier.

B. Receive Signal Model

We consider a two-dimensional coordinate system for the near-field sensing system, as illustrated in Fig. 1. The origin of the coordinate system is put into the center of the UCA at the BS. For the target, let r and θ denote its distance from the origin and the angle with respect to the x -axis. Then, the coordinate of the target can be expressed as $\mathbf{r} = [r \cos \theta, r \sin \theta]^T$. Let d denote the antenna spacing of the UCA at the BS. The radius of the UCA is thus given by $R = \frac{Nd}{2\pi}$, which satisfies $R \leq r$. In this case, the coordinate \mathbf{s}_n of the n -th antenna can be expressed as $\mathbf{s}_n = [R \cos \psi_n, R \sin \psi_n]^T$, where $\psi_n = \frac{2\pi n}{N}$. The near-field propagation distance of the signal from the n -th antenna to the target is given by [6]

$$r_n = \|\mathbf{r} - \mathbf{s}_n\| = \sqrt{r^2 + R^2 - 2rR \cos(\theta - \psi_n)}. \quad (2)$$

Given the propagation distance, the round-trip propagation delay $\tau_{n,i}$ of the echo signal from the n -th antenna to the i -th antenna at the BS is $\tau_{n,i} = (r_n + r_i)/c$, where c denotes the speed of light. Let $\bar{\mathbf{x}}_n(t) = [\bar{\mathbf{x}}(t)]_n$ denote the baseband signals transmitted by the n -th antenna of the UCA. The duration of CP is assumed to be larger than the largest round-trip delay of the target. Then, the noiseless continuous-time baseband echo signal received at the i -th antenna at the UCA is given by [15]

$$y_i(t) = \sum_{n=1}^N \beta \bar{\mathbf{x}}_n(t - \tau_{n,i}) e^{-j2\pi f_c \tau_{n,i}} \quad (3)$$

where β is a complex channel gain including the round-trip pathloss and radar cross section. Then, sampling $s_i(t)$ at time $t = lT_{\text{tot}} + T_{\text{cp}} + k\frac{T_s}{M}$ for $k = 0, \dots, M-1$ and omitting the constant terms yields the following discrete-time signal model in the l -th OFDM symbol after removing CP [14]:

$$\begin{aligned} y_{l,i}[k] &= \frac{1}{\sqrt{M}} \sum_{n=1}^N \sum_{m=0}^{M-1} \beta x_{l,m,n} e^{j2\pi \delta_m \Delta f (\frac{kT_s}{M} - \tau_{n,i})} e^{-j2\pi f_c \tau_{n,i}} \\ &= \frac{1}{\sqrt{M}} \sum_{n=1}^N \sum_{m=0}^{M-1} \beta x_{l,m,n} e^{-j2\pi f_m \tau_{n,i}} e^{j2\pi \frac{m k}{M}}, \end{aligned} \quad (4)$$

where $x_{l,m,n}$ denotes the n -th entry of vector $\mathbf{x}_{l,m}$ and $f_m = f_c + \delta_m \Delta f$ is the frequency of the m -th subcarrier. The receive signal vector $\mathbf{y}_l[k] = [y_{l,1}[k], \dots, y_{l,N}[k]]^T$ is thus given by

$$\mathbf{y}_l[k] = \frac{1}{\sqrt{M}} \sum_{m=0}^{M-1} \beta \mathbf{a}_m^*(r, \theta) \mathbf{a}_m^H(r, \theta) \mathbf{x}_{l,m} e^{j2\pi \frac{m k}{M}}, \quad (5)$$

where $\mathbf{a}(r, \theta) \in \mathbb{C}^{N \times 1}$ is known as the near-field array response vector at frequency f_m and is given by

$$\mathbf{a}_m(r, \theta) = [e^{-jk_m r_1}, \dots, e^{-jk_m r_N}]^H, \quad (6)$$

with $k_m = \frac{2\pi f_m}{c}$ denoting the wavenumber. Then, the noisy signal received on the m -th subcarrier in the l -th OFDM symbol can be obtained by DFT as follows

$$\begin{aligned} \mathbf{y}_{l,m} &= \text{DFT}(\mathbf{y}_l[k])_m + \mathbf{z}_{l,m} \\ &= \beta \mathbf{a}_m^*(r, \theta) \mathbf{a}_m^H(r, \theta) \mathbf{x}_{l,m} + \mathbf{z}_{l,m}, \end{aligned} \quad (7)$$

where $\mathbf{z}_{l,m}$ denote the additive white Gaussian noise with each entry obeying $\mathcal{CN}(0, \sigma^2)$. Aggregating $\mathbf{y}_{l,m}$ over L OFDM symbols yields

$$\mathbf{Y}_m = [\mathbf{y}_{1,m}, \dots, \mathbf{y}_{L,m}] = \beta \mathbf{A}_m(r, \theta) \mathbf{X}_m + \mathbf{Z}_m, \quad (8)$$

where $\mathbf{A}_m(r, \theta) = \mathbf{a}_m^*(r, \theta) \mathbf{a}_m^H(r, \theta)$, $\mathbf{X}_m = [\mathbf{x}_{1,m}, \dots, \mathbf{x}_{L,m}]$, and $\mathbf{Z}_m = [\mathbf{z}_{1,m}, \dots, \mathbf{z}_{L,m}]$. In the mono-static sensing setup, the data signal \mathbf{X}_m is known at the BS. Therefore, the problem for near-field sensing is to estimate the remaining unknown parameters, i.e., complex channel gain β , distance r , and angle θ , related to the targets from the receive signals $\{\mathbf{Y}_m\}_{m=0}^{M-1}$ in (8) based on the knowledge of \mathbf{X}_m . We focus primarily on the estimation of r and θ , i.e., the location information of the target.

III. PERFORMANCE BOUNDS AND ANALYSIS

In this section, the performance bounds for angle and distance estimation are characterized and analyzed. In particular, the most popular CRB is considered, which provides a tight lower bound of mean-squared error for unbiased estimators under some general and mild conditions [8]–[11].

A. Cramér-Rao Bound

We now derive the CRBs for estimating r and θ from the signals $\{\mathbf{Y}_m\}_{m=0}^{M-1}$. To this end, we first stack the signals $\{\mathbf{Y}_m\}_{m=0}^{M-1}$ a single vector as follows:

$$\mathbf{y} = \underbrace{\begin{bmatrix} \text{vec}(\beta \mathbf{A}_0(r, \theta) \mathbf{X}_0) \\ \vdots \\ \text{vec}(\beta \mathbf{A}_{M-1}(r, \theta) \mathbf{X}_{M-1}) \end{bmatrix}}_{\mathbf{u}} + \begin{bmatrix} \text{vec}(\mathbf{Z}_0) \\ \vdots \\ \text{vec}(\mathbf{Z}_{M-1}) \end{bmatrix}. \quad (9)$$

Following the results in [11], we define vectors $\mathbf{u}_\theta = \frac{\partial \mathbf{u}}{\partial \theta}$ and $\mathbf{u}_r = \frac{\partial \mathbf{u}}{\partial r}$, and the following matrix

$$\mathbf{Q} = \begin{bmatrix} \|\mathbf{u}_\theta\|^2 \sin^2 \Omega & \frac{\text{Re}\{\mathbf{u}_\theta^H \Phi \mathbf{u}\}}{\|\mathbf{u}\|^2} \\ \frac{\text{Re}\{\mathbf{u}_r^H \Phi \mathbf{u}\}}{\|\mathbf{u}\|^2} & \|\mathbf{u}_r\|^2 \sin^2 \Theta \end{bmatrix}, \quad (10)$$

where $\sin^2 \Omega = 1 - \frac{|\mathbf{u}_\theta^H \mathbf{u}|^2}{\|\mathbf{u}_\theta\|^2 \|\mathbf{u}\|^2}$, $\sin^2 \Theta = 1 - \frac{|\mathbf{u}_r^H \mathbf{u}|^2}{\|\mathbf{u}_r\|^2 \|\mathbf{u}\|^2}$, and $\Phi = \mathbf{u}_\theta^H \mathbf{u}_r \mathbf{I} - \mathbf{u}_\theta \mathbf{u}_r^H$. Then, the CRBs for estimating θ and r can be respectively calculated by [11]

$$\text{CRB}_\theta = \frac{\sigma^2 \|\mathbf{u}_r\|^2 \sin^2 \Theta}{2 \det \mathbf{Q}}, \quad \text{CRB}_r = \frac{\sigma^2 \|\mathbf{u}_\theta\|^2 \sin^2 \Omega}{2 \det \mathbf{Q}}. \quad (11)$$

It can be observed that the value of CRBs is determined by the following intermediate parameters: $u = \|\mathbf{u}\|^2$, $u_\theta = \|\mathbf{u}_\theta\|^2$, $u_r = \|\mathbf{u}_r\|^2$, $c_\theta = \mathbf{u}_\theta^H \mathbf{u}$, $c_r = \mathbf{u}_r^H \mathbf{u}$, and $\eta = \mathbf{u}_\theta^H \mathbf{u}_r$. Specifically, the expression of u is given by

$$u = \sum_{m=0}^{M-1} \|\text{vec}(\beta \mathbf{A}_m(r, \theta) \mathbf{X}_m)\|^2 \approx \sum_{m=0}^{M-1} |\beta|^2 L \text{tr}(\mathbf{A}_m(r, \theta) \mathbf{R}_m \mathbf{A}_m(r, \theta)^H), \quad (12)$$

where (a) stems from the equality $\|\text{vec}(\mathbf{X})\|^2 = \text{tr}(\mathbf{X}\mathbf{X}^H)$ and the approximation $\frac{1}{L} \mathbf{X}_m \mathbf{X}_m^H \approx \mathbb{E}[\mathbf{x}_{l,m} \mathbf{x}_{l,m}^H] = \mathbf{R}_m$. This approximation is valid under the condition of a sufficiently large value for L . Consequently, we assume that the accurate equality of them holds true throughout this paper. Furthermore, parameter u can be rewritten as a function of the beamforming gain. In particular, given the transmit covariance matrix, the beamforming gain at the target location on the m -th subcarrier is $G_m = \mathbf{a}_m^H(r, \theta) \mathbf{R}_m \mathbf{a}_m(r, \theta)$. It is easy to prove that $0 \leq G_m \leq NP$, where the maximum value is achieved when $\mathbf{R}_m = \frac{P}{N} \mathbf{a}_m(r, \theta) \mathbf{a}_m^H(r, \theta)$. For brevity, we assume $G_0 = \dots = G_{M-1} \triangleq G$. Thus, the parameter u can be rewritten as

$$u \approx \sum_{m=0}^{M-1} |\beta|^2 L G \text{tr}(\mathbf{a}_m^*(r, \theta) \mathbf{a}_m^T(r, \theta)) = |\beta|^2 L G N M. \quad (13)$$

Furthermore, to calculate the intermediate parameters involving \mathbf{u}_θ and \mathbf{u}_r , we first define the following derivatives:

$$\dot{\mathbf{G}}_{\theta, m} \triangleq \frac{\partial \mathbf{A}_m(r, \theta)}{\partial \theta} = -2j k_m \Theta \mathbf{A}_m(r, \theta), \quad (14)$$

$$\dot{\mathbf{G}}_{r, m} \triangleq \frac{\partial \mathbf{A}_m(r, \theta)}{\partial r} = -2j k_m \Upsilon \mathbf{A}_m(r, \theta), \quad (15)$$

where Θ and Υ are diagonal matrices whose n -th diagonal entries are $[\Theta]_{n,n} = \frac{\partial r_n}{\partial \theta}$ and $[\Upsilon]_{n,n} = \frac{\partial r_n}{\partial r}$, respectively. Then, \mathbf{u}_θ and \mathbf{u}_r can be reformulated as

$$\mathbf{u}_i = \begin{bmatrix} \text{vec}(\beta \dot{\mathbf{G}}_{i,0} \mathbf{X}_0) \\ \vdots \\ \text{vec}(\beta \dot{\mathbf{G}}_{i,M-1} \mathbf{X}_{M-1}) \end{bmatrix}, \quad \forall i \in \{\theta, r\}. \quad (16)$$

Then, following the similar process as (12), the expressions of the intermediate parameter u_θ is given by

$$u_\theta = \sum_{m=0}^{M-1} 4|\beta|^2 L k_m^2 \text{tr}(\Theta \mathbf{A}_m(r, \theta) \mathbf{R}_m \mathbf{A}_m^H(r, \theta) \Theta^H) = 4|\beta|^2 k_0^2 L G \tilde{M} \tilde{u}_\theta, \quad (17)$$

where $k_0 = \frac{2\pi}{c}$, $\tilde{M} = \sum_{m=0}^{M-1} f_m^2$, and $\tilde{u}_\theta = \sum_{n=1}^N \left(\frac{\partial r_n}{\partial \theta}\right)^2$. Similarly, it can be shown that

$$u_r = 4|\beta|^2 k_0^2 L G \tilde{M} \tilde{u}_r, \quad c_\theta = -2j|\beta|^2 k_0 L G \tilde{M} \tilde{c}_\theta, \quad (18)$$

$$c_r = -2j|\beta|^2 k_0 L G \tilde{M} \tilde{c}_r, \quad \eta = 4|\beta|^2 k_0^2 L G \tilde{M} \tilde{\eta}, \quad (19)$$

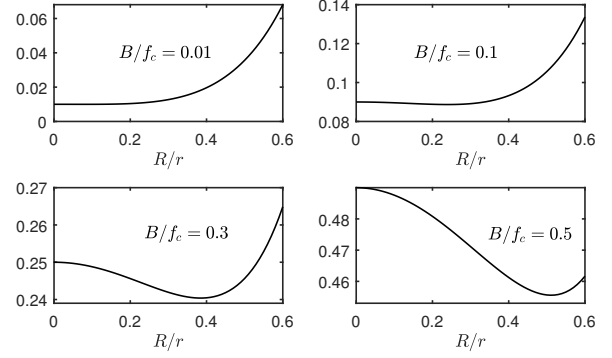


Fig. 2: The numerical results of function $\Xi\left(\frac{R}{r}, \frac{B}{f_c}\right)$.

where $\tilde{u}_r = \sum_{n=1}^N \left(\frac{\partial r_n}{\partial r}\right)^2$, $\tilde{c}_\theta = \sum_{n=1}^N \frac{\partial r_n}{\partial \theta}$, $\tilde{c}_r = \sum_{n=1}^N \frac{\partial r_n}{\partial r}$, $\tilde{\eta} = \sum_{n=1}^N \frac{\partial r_n}{\partial \theta} \frac{\partial r_n}{\partial r}$, and $\tilde{M} = \sum_{m=0}^{M-1} f_m$. To obtain the closed-form expressions of the CRBs, we first derive the following lemma.

Lemma 1. If $N \gg 1$ and $R \leq r$, the closed-form expressions of \tilde{u}_θ , \tilde{u}_r , \tilde{c}_θ , \tilde{c}_r , $\tilde{\eta}$, \tilde{M} , and \bar{M} can be derived as

$$\tilde{u}_\theta = \frac{R^2 N}{2}, \quad \tilde{u}_r = N - \frac{R^2 N}{2r^2}, \quad \tilde{c}_r = NK \left(\frac{r}{R}\right), \quad \tilde{c}_\theta = 0, \\ \tilde{\eta} = 0, \quad \tilde{M} = M f_c^2 + \frac{M(M^2 - 1)}{12} \Delta f^2, \quad \bar{M} = M f_c, \quad (20)$$

where $K(\alpha)$ is a transcendental function given by

$$K(\alpha) = \int_0^{2\pi} \frac{\alpha - \cos x}{2\pi \sqrt{1 - 2\alpha \cos x + \alpha^2}} dx. \quad (21)$$

Proof: Please refer to the Appendix. \blacksquare

Based on the results in **Lemma 1**, the closed-form expression of the intermediate parameters in (17)-(19) can be obtained. By substituting them into (11), the closed-form CRBs can be obtained, given in the following theorem.

Theorem 1. The closed-form CRBs achieved by UCAs when $R \leq r$ are given by

$$\text{CRB}_\theta = \frac{3\sigma^2}{\rho L N M R^2 (12f_c^2 + B^2 - \Delta f^2)}, \quad (22)$$

$$\text{CRB}_r = \frac{3\sigma^2}{\left(2\rho L N M \left[12f_c^2 \left(1 - \frac{R^2}{2r^2} - K^2\left(\frac{r}{R}\right)\right) + (B^2 - \Delta f^2) \left(1 - \frac{R^2}{2r^2}\right)\right]\right)}, \quad (23)$$

where $\rho = k_0^2 |\beta|^2 G$ is related to the channel gain and beamforming gain, $R = \frac{Nd}{2\pi}$ is the radius (half of the aperture) of the UCA, and $B = M\Delta f$ is the signal bandwidth.

In **Theorem 1**, it can be observed that CRB_r is inversely proportional to the following function:

$$\Xi\left(\frac{R}{r}, \frac{B}{f_c}\right) = 12 \left(1 - \frac{R^2}{2r^2} - K^2\left(\frac{r}{R}\right)\right) + \frac{B^2 - \Delta f^2}{f_c^2} \left(1 - \frac{R^2}{2r^2}\right). \quad (24)$$

The behavior of this function when $M \gg 1$, i.e., $B^2 - \Delta f^2 \approx B^2$ is illustrated in Fig. 2. From the closed-form expressions of CRBs in **Theorem 1** and the results in Fig. 2, we notice the following (keeping in mind $R \leq r$, $N \gg 1$, and $M \gg 1$).

- **Robustness of UCA:** CRB_θ and CRB_r achieved by UCA is independent of the angle of the target θ . This is fundamentally different from the conventional ULAs with an angular-dependent performance [8]–[11]. Therefore, UCAs can provide more stable performance than ULAs.
- **Impact of Bandwidth:** Both CRB_θ and CRB_r are $O(1/M)$ and decrease with both larger carrier frequency f_c and bandwidth B . Compared to CRB_r , CRB_θ is less affected by the bandwidth B . This is because the $(12f_c^2 + B^2 - \Delta f^2)$ term in its denominator is mainly affected by $12f_c^2$ unless $B^2 - \Delta f^2$ has a comparable value to $12f_c^2$, which is impossible in practice. In contrast, CRB_r is significantly affected by the bandwidth B , which will be detailed in the sequel.
- **Impact of Array Size:** CRB_θ is $O(1/N)$ and $O(1/R^2)$ but is independent of r . This suggests that increasing the array aperture is more advantageous for angle estimation than increasing the number of antennas. If the antenna spacing d remains constant, the radius R is proportional to the number of antennas, where $R = \frac{Nd}{2\pi}$. In this case, CRB_θ is $O(1/N^3)$. On the contrary, CRB_r is $O(1/N)$ but exhibits a more complex dependence R and r , characterized by the function $\Xi(\frac{R}{r}, \frac{B}{f_c})$ in (24). According to the results in Fig. 2, larger array apertures or closer targets (i.e., a larger ratio of R/r) generally enhance the performance of distance estimation with the practical ratio B/f_c less than 0.1. However, this trend appears to reverse at ultra-high values of B/f_c , exceeding 0.3, where larger apertures or closer targets may actually degrade the performance of distance estimation. It is important to note that such high values of B/f_c are generally uncommon in practice.
- **Impact of Beamforming:** Both CRB_θ and CRB_r are $O(1/G)$. Recall that the beamforming gain G varies between 0 and NP , achieving its maximum when $\mathbf{R}_m = \frac{P}{N} \mathbf{a}_m(r, \theta) \mathbf{a}_m^H(r, \theta), \forall m$. At this maximum, both CRB_θ and CRB_r are reduced to $O(1/N^2)$. Moreover, if the antenna spacing d remains constant, CRB_θ can further decrease to $O(1/N^4)$ under maximum G . However, attaining the maximum G necessitates prior knowledge of r and θ , which is typically unavailable in practice. As an alternative, isotropic beamforming provides a robust solution for unknown target locations, defined by $\mathbf{R}_m = \frac{P}{N} \mathbf{I}_N, \forall m$ [16]. This method results in a constant beamforming gain of $G = P$, independent of N .
- **Origins of Performance Gain:** In the considered system, the total number of observations for target sensing is LMN , where L , M , and N denote the number of observations collected across the time, frequency, and space domains, respectively. Recall that with fixed G , R , and B , both CRB_θ and CRB_r are $O(1/N)$ and

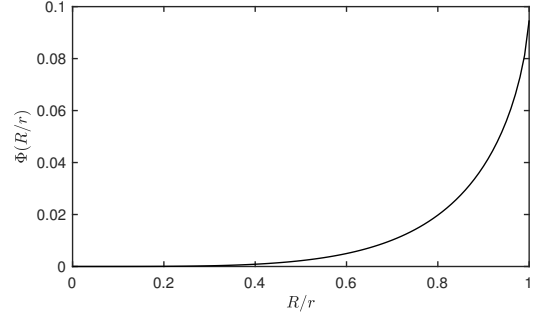


Fig. 3: The numerical results of function $\Phi(\frac{R}{r})$.

$O(1/M)$. This suggests that when the array aperture and signal bandwidth remain constant, the performance gain from adding more antennas and subcarriers stems solely from the increase in the total number of observations, rather than changing the near-field and wideband effects. Conversely, modifications to the array aperture or signal bandwidth directly impact these effects, thereby fundamentally altering sensing performance.

B. Asymptotic CRBs

In this subsection, we dive further into the asymptotic behavior of CRBs to obtain more insights. Based on the **Theorem 1**, it is easy to prove the following corollaries.

Corollary 1. As $r \rightarrow \infty$, the asymptotic CRB_r satisfies

$$\lim_{r \rightarrow \infty} \text{CRB}_r = \frac{3\sigma^2}{2\rho LNM (B^2 - \Delta f^2)}. \quad (25)$$

Proof: As $r \rightarrow \infty$, we have $\lim_{r \rightarrow \infty} \frac{R}{2r^2} = 0$ and

$$\lim_{r \rightarrow \infty} K\left(\frac{r}{R}\right) = \lim_{\alpha \rightarrow \infty} K(\alpha) = \int_0^{2\pi} \frac{1}{2\pi} dx = 1. \quad (26)$$

By substituting these two limits into (23), the expression in (25) can be obtained. ■

Corollary 2. As $M \rightarrow 1$, the asymptotic CRB_r satisfies

$$\lim_{M \rightarrow 1} \text{CRB}_r = \frac{\sigma^2}{8\rho L N f_c^2 \left(1 - \frac{R^2}{2r^2} - K^2\left(\frac{r}{R}\right)\right)}. \quad (27)$$

Proof: As $M \rightarrow 1$, we have $B = \Delta f$, thus $B^2 - \Delta f^2 = 0$. Substituting this result into (23) yields (27). ■

Corollary 3. As $r \rightarrow \infty$ and $M \rightarrow 1$, the asymptotic CRB_r satisfies

$$\lim_{r \rightarrow \infty, M \rightarrow 1} \text{CRB}_r = \infty. \quad (28)$$

Proof: The above results can be readily obtained according to **Corollaries 1 and 2**. ■

According to **Corollary 2**, in the single-carrier system, the CRB_r is inversely proportional to the following function:

$$\Phi\left(\frac{R}{r}\right) = 1 - \frac{R^2}{2r^2} - K^2\left(\frac{r}{R}\right), \quad (29)$$

The behavior of this function is illustrated in Fig. 3. From the asymptotic CRBs in **Corollaries 1-3** and the results in Fig. 3, we notice the following additional insights.

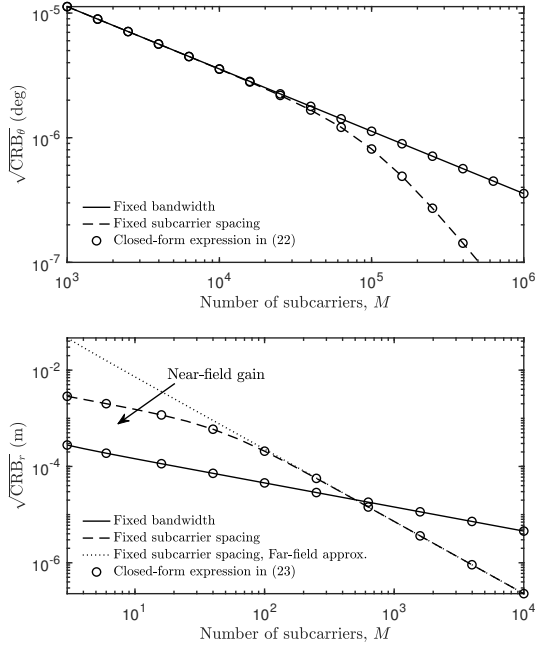


Fig. 4: CRBs versus the number of subcarriers under the conditions of the fixed bandwidth of $B = 500$ MHz and the fixed subcarrier spacing of 1 MHz, respectively.

- **Corollary 1** presents CRB_r in *far-field systems*, where $r \rightarrow \infty$. In far-field systems, when the number of observations $LN M$ remains constant, CRB_r is merely related to the bandwidth B . This finding aligns with previous research on far-field sensing [7].
- **Corollary 2** describes CRB_r in *single-carrier systems*. According to the results in Fig. 3, a larger array aperture or a closer target (i.e., a larger ratio of R/r) can always lead to a better performance of distance estimation. This result is consistent with the existing studies on single-carrier near-field sensing [8]–[11].
- **Corollary 3** explores CRB_r in *single-carrier far-field systems*. In this scenario, we have $\text{CRB}_r = \infty$. This suggests an unbounded estimation error, rendering distance estimation infeasible under these conditions.

IV. NUMERICAL RESULTS

In this section, numerical results are provided to validate the analytical results. Unless otherwise specified, we set $r = 20$ m, $\theta = 90^\circ$, $f_c = 30$ GHz, $B = 10$ MHz, $L = 256$, $M = 256$, $N = 256$, $R = 0.5$ m, and $\frac{|\beta|^2 P}{\sigma^2} = 0$ dB.

Fig. 4 examines the influence of bandwidth on sensing performance under two different conditions: fixed bandwidth and fixed subcarrier spacing. In the case of fixed bandwidth, increasing the number of subcarriers only leads to more observation samples. Conversely, in the fixed subcarrier spacing scenario, increasing the number of subcarriers also expands the bandwidth. From Fig. 4(a), it can be observed that for angle estimation, increasing bandwidth has a marginal effect on its accuracy unless the bandwidth is extremely large, e.g., when $M \geq 10^5$ with 1 MHz subcarrier spacing. In this

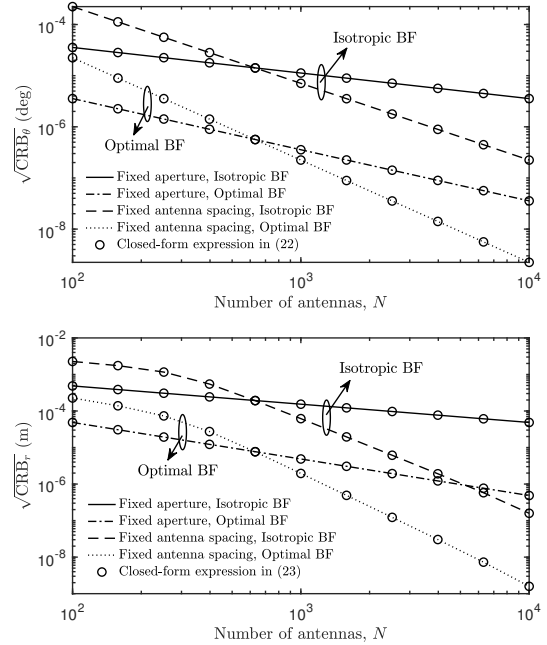


Fig. 5: CRBs versus the number of antennas under the conditions of the fixed aperture of $R = 0.5$ m and the fixed antenna spacing of $d = \frac{c}{2f_c}$, respectively.

case, the bandwidth is $B = 10^5 \times 1$ MHz = 100 GHz. This bandwidth is much larger than the carrier frequency f_c , which is impossible. Therefore, in practice system setup with $B \ll f_c$, bandwidth has negligible impact on angle estimation. Furthermore, for distance estimation, bandwidth has a much more significant impact, leading to a faster decrease in CRB. Furthermore, it reveals that the near-field gain in distance estimation is substantial when the bandwidth is small, but becomes negligible when the bandwidth is extremely large.

Fig. 5 explores the impact of array size on sensing performance with either fixed aperture or fixed antenna spacing under different beamforming (BF) strategies. For fixed aperture, more antennas only lead to more observation samples. For fixed antenna spacing, more antennas also enlarge the array aperture, thus enhancing the near-field effect. It can be observed that the CRBs for angle and distance estimation exhibit similar trends as the number of antennas N increases. First, both angle and distance estimation derive greater benefits from larger array apertures rather than merely increasing the number of antennas. Second, both metrics significantly improve with appropriate beamforming optimization.

Fig. 6 explores the effect of target distance on the accuracy of distance estimation across different aperture and bandwidth configurations. There are two key observations. First, the accuracy of distance estimation approaches the far-field bound more rapidly with larger bandwidths, indicating that a larger bandwidth diminishes the extent of the near-field effect. Second, when the target distance is relatively moderate (e.g., $r \leq 60$ m), expanding the array aperture (without the addition of more antennas) is more advantageous than increasing the bandwidth, without incurring additional hardware costs or

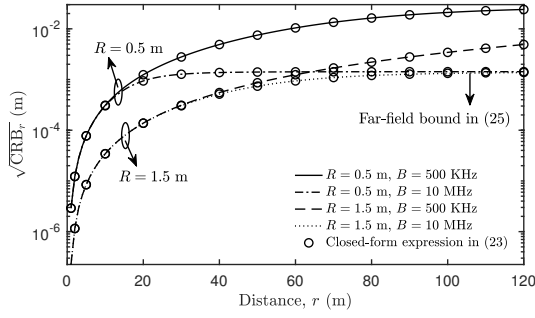


Fig. 6: CRBs versus the target's distance under the conditions of different array apertures and signal bandwidths.

using more spectrum resources.

V. CONCLUSION

This paper studied the joint impact of bandwidth and array size on near-field sensing with circular arrays based on the CRB framework. The developed results suggested a highly coupled relationship between bandwidth and array size for the sensing performance. The developed results also included the existing results as special cases, providing a more accurate model for performance evaluation in practice.

APPENDIX

For UCAs, partial derivatives of the propagation distance r_n with respect to r and θ are given by

$$\frac{\partial r_n}{\partial \theta} = \frac{rR \sin(\theta - \frac{2\pi n}{N})}{\sqrt{r^2 + R^2 - 2rR \cos(\theta - \frac{2\pi n}{N})}}, \quad (30)$$

$$\frac{\partial r_n}{\partial r} = \frac{r - R \cos(\theta - \frac{2\pi n}{N})}{\sqrt{r^2 + R^2 - 2rR \cos(\theta - \frac{2\pi n}{N})}}. \quad (31)$$

By defining $\delta = \frac{2\pi}{N}$, the parameter \tilde{u}_θ can be derived as

$$\begin{aligned} \tilde{u}_\theta &= \sum_{n=1}^N \left(\frac{\partial r_n}{\partial \theta} \right)^2 = \sum_{n=1}^N \frac{r^2 R^2 \sin^2(\theta - \frac{2\pi n}{N})}{r^2 + R^2 - 2rR \cos(\theta - \frac{2\pi n}{N})} \\ &= \frac{r^2 R^2}{\delta} \sum_{n=1}^N \frac{\sin^2(\theta - n\delta)}{r^2 + R^2 - 2rR \cos(\theta - n\delta)} \delta \\ &\stackrel{(a)}{\approx} \frac{r^2 R^2 N}{2\pi} \int_0^{2\pi} \frac{\sin^2 x}{r^2 + R^2 - 2rR \cos x} dx \\ &= \frac{r^2 R^2 N}{2\pi} \left(\int_0^\pi \frac{\sin^2 x}{r^2 + R^2 - 2rR \cos x} dx \right. \\ &\quad \left. + \int_0^\pi \frac{\sin^2 x}{r^2 + R^2 + 2rR \cos x} dx \right) \stackrel{(b)}{=} \frac{R^2 N}{2}, \quad (32) \end{aligned}$$

where approximation (a) is obtained based on $\delta \ll 1$ when $N \gg 1$ and step (b) is derived based on the integral formula [17, Eq. (3.613.3)] when $R \leq r$. Similarly, the remaining parameters can be derived as follows:

$$\tilde{u}_r = N - \frac{1}{r^2} \tilde{u}_\theta \approx N - \frac{R^2 N}{2r^2}, \quad (33)$$

$$\tilde{c}_\theta \approx \int_0^{2\pi} \frac{rRN \sin x}{2\pi \sqrt{r^2 + R^2 - 2rR \cos x}} dx \stackrel{(c)}{=} 0, \quad (34)$$

$$\tilde{c}_r \approx \int_0^{2\pi} \frac{N(r - R \cos x)}{2\pi \sqrt{r^2 + R^2 - 2rR \cos x}} dx = NK \left(\frac{r}{R} \right), \quad (35)$$

$$\tilde{\eta} \approx \int_0^{2\pi} \frac{rRN(R \sin x \cos x - r \sin x)}{2\pi(r^2 + R^2 - 2rR \cos x)} dx \stackrel{(d)}{=} 0, \quad (36)$$

where steps (c) and (d) are obtained according to the symmetry property of the functions and function $K(\alpha)$ is given by

$$K(\alpha) = \int_0^{2\pi} \frac{\alpha - \cos x}{2\pi \sqrt{1 - 2\alpha \cos x + \alpha^2}} dx. \quad (37)$$

It can be proved that the function $K(\alpha)$ is a transcendental function that does not have a closed-form expression. Moreover, recall $f_m = f_c + \delta_m \Delta f$, with $\delta_m = \frac{2m-M+1}{2}$. Thus, the parameters of \tilde{M} and \bar{M} can be derived as follows

$$\tilde{M} = \sum_{m=0}^{M-1} f_m^2 = M f_c^2 + \frac{M(M^2 - 1)}{12} \Delta f^2, \quad (38)$$

$$\bar{M} = \sum_{m=0}^{M-1} f_m = M f_c. \quad (39)$$

The proof of Lemma 1 is thus completed.

REFERENCES

- [1] E. Fishler *et al.*, "MIMO radar: An idea whose time has come," in *Proc. IEEE Radar Conf.*, Apr. 2004, pp. 71–78.
- [2] F. Liu *et al.*, "Integrated sensing and communications: Toward dual-functional wireless networks for 6G and beyond," *IEEE J. Sel. Areas Commun.*, vol. 40, no. 6, pp. 1728–1767, Jun. 2022.
- [3] T. L. Marzetta, "Noncooperative cellular wireless with unlimited numbers of base station antennas," *IEEE Trans. Wireless Commun.*, vol. 9, no. 11, pp. 3590–3600, Nov. 2010.
- [4] E. Björnson *et al.*, "Massive MIMO is a reality—what is next?: Five promising research directions for antenna arrays," *Digit. Signal Process.*, vol. 94, pp. 3–20, Nov. 2019.
- [5] Z. Wang *et al.*, "A tutorial on extremely large-scale MIMO for 6G: Fundamentals, signal processing, and applications," *IEEE Commun. Surv. Tut.*, 2024.
- [6] Y. Liu *et al.*, "Near-field communications: A tutorial review," *IEEE Open J. Commun. Soc.*, vol. 4, pp. 1999–2049, Aug. 2023.
- [7] J. Guerci, R. Guerci, A. Lackpour, and D. Moskowitz, "Joint design and operation of shared spectrum access for radar and communications," in *Proc. IEEE Radar Conf.*, 2015, pp. 761–766.
- [8] M. N. El Korso, R. Boyer, A. Renaux, and S. Marcos, "Conditional and unconditional Cramér–rao bounds for near-field source localization," *IEEE Trans. Signal Process.*, vol. 58, no. 5, pp. 2901–2907, May 2010.
- [9] L. Khamidullina *et al.*, "Conditional and unconditional Cramér–rao bounds for near-field localization in bistatic MIMO radar systems," *IEEE Trans. Signal Process.*, vol. 69, pp. 3220–3234, May 2021.
- [10] Z. Wang, X. Mu, and Y. Liu, "Near-field integrated sensing and communications," *IEEE Communications Letters*, 2023.
- [11] H. Wang, Z. Xiao, and Y. Zeng, "Cramér–Rao bounds for near-field sensing with extremely large-scale MIMO," *IEEE Trans. Signal Process.*, vol. 72, pp. 701–717, Jan. 2024.
- [12] Z. Wu, M. Cui, and L. Dai, "Enabling more users to benefit from near-field communications: From linear to circular array," *IEEE Trans. Wireless Commun.*, vol. 23, no. 4, pp. 3735–3748, Apr. 2024.
- [13] Z. Wang, X. Mu, and Y. Liu, "Rethinking integrated sensing and communication: When near field meets wideband," *IEEE Commun. Mag.*, accepted to appear, 2024.
- [14] C. Sturm and W. Wiesbeck, "Waveform design and signal processing aspects for fusion of wireless communications and radar sensing," *Proc. IEEE*, vol. 99, no. 7, pp. 1236–1259, Jul. 2011.
- [15] D. Tse and P. Viswanath, *Fundamentals of wireless communication*. Cambridge, U.K.: Cambridge Univ. Press, 2005.
- [16] P. Stoica, J. Li, and Y. Xie, "On probing signal design for MIMO radar," *IEEE Trans. Signal Process.*, vol. 55, no. 8, pp. 4151–4161, Aug. 2007.
- [17] I. S. Gradshteyn and I. M. Ryzhik, *Table of Integrals, Series, and Products*. San Diego, C.A., USA: Academic, 2007.